Research Article

Terahertz Absorption Characteristics of Multiwalled Carbon Nanotube Aqueous Dispersion Measured by Microfluidic Technique

Yuchai Li [iD],[1] Siyu Qian [iD],[1,2,3,4] Hangyu Zhou [iD],[1] Huimin Jiang [iD],[1] Xue Wang [iD],[1] Bo Su [iD],[1,2,3,4] and Cunlin Zhang [iD][1,2,3,4]

[1]*Department of Physics, Capital Normal University, Beijing 100048, China*
[2]*Key Laboratory of THz Optoelectronics, Ministry of Education, Beijing 100048, China*
[3]*Beijing Key Laboratory of THz Spectroscopy and Imaging, Beijing 100048, China*
[4]*Beijing Advanced Innovation Center for Imaging Theory and Technology, Beijing 100048, China*

Correspondence should be addressed to Bo Su; subo75@cnu.edu.cn

Multiwalled carbon nanotubes (MWCNTs) have excellent electronic, mechanical, and structural characteristics; however, their poor dispersion structure and large aggregates severely inhibit their function. A stable MWCNT dispersion in an aqueous solvent has been realized via ultrasonic dispersion and surfactant modification, providing a reference for improving MWCNT dispersion in various materials and solvents. In this study, a cyclic olefin copolymer with high transmittance to terahertz (THz) waves is used to prepare microfluidic chips. Then, the microfluidic and THz technologies are combined to study the THz absorption characteristics of MWCNT aqueous dispersion under different electric field (EF) intensities, magnetic field (MF) intensities, and MF action time. The results show that the THz spectral intensity of MWCNT aqueous dispersion decreases and the absorption coefficient increases with the increase of EF intensity, MF intensity, and MF action time. This phenomenon is explained from a microscopic perspective. The combination of microfluidic and THz technologies provides technical support for studying the characteristics of MWCNT aqueous dispersion and lays a foundation for elucidating the molecular microstructure of MWCNT aqueous dispersion.

1. Introduction

Terahertz (THz) waves are electromagnetic waves with frequency and wavelength ranges of 0.1–10 THz and 30–3,000 μm, respectively. THz time-domain spectroscopy (THz-TDS) is a mature technology, which not only can directly obtain signal amplitude and phase with a high signal-to-noise ratio (greater than 60 dB) [1]. THz absorbing materials are essential in the field of national security and information protection as well as having application potential in communications [2], signal modulation [3], imaging [4], and sensing [5]. In addition, ultrathin wideband THz absorbing techniques are effective means to realize high sensitivity and fast wideband THz

detection [6]. In recent years, researchers have designed a series of tunable THz absorbers [7–11], which can achieve narrow-band, wideband, double band, and multiband absorption. This has aroused great interest and become a research hotspot. From the perspective of absorption bandwidth and absorption intensity, the specific average THz absorption performance of multiwalled carbon nanotube (MWCNT) is achieved up to 3.6×10^4 dB·cm³·g⁻¹, which is over thousands of times larger than other kinds of materials reported previously [12]. In 2020, Gorokhov et al. [13] fabricated lightweight and compact MWCNT-basedmeta-surfaces, which are able to replace conventional pyramidal absorbers and have been shown to serve as a versatile platform for scalable cost-
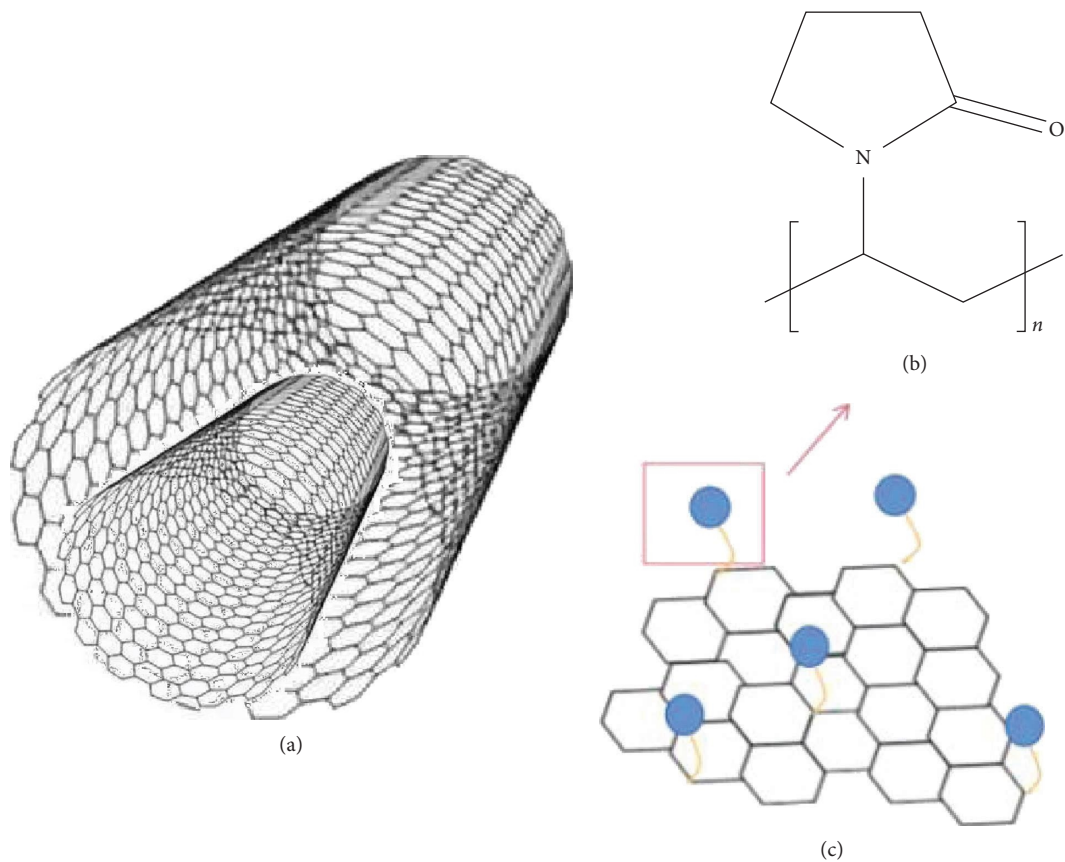
Figure 1: (a) Structure of MWCNT, (b) PVP molecular formula, and (c) a schematic of chemical grafting reaction between PVP and MWCNT.

efficient production of ultra-light electromagnetic components for THz applications. However, the strong van der Waals forces between carbon nanotubes (CNTs), their large specific surface areas, and high aspect ratios make them easy to agglomerate or wind [14]. Moreover, the lack of active groups on CNT surfaces results in their poor dispersion in various solvents [15]. At present, CNT dispersion technology is reaching maturity; however, the research on CNT dispersion in water is still inadequate.

MWCNTs comprise a group of single-walled CNTs with different radii arranged coaxially (Figure 1) [16]. The outer diameter of MWCNTs depends on the growth process and is generally within 20–100 nm [17]. The MWCNT/surfactant aqueous dispersion comprises MWCNTs, surfactant PVP, and water. The molecular formula of PVP is $(C_6H_9NO)_n$, which is an amphiphilic polymer. The pyrrolidone group of PVP is hydrophilic, and its main chain is a hydrophobic carbon–carbon bond segment. In addition, in MWCNT aqueous dispersion, a chemical grafting reaction between PVP and MWCNTs occurs [18].

Microfluidic technologies use micron-scale channels to manipulate a very small volume of fluid. A very small sample volume can provide a large amount of useful data, such as analytical parameters. Recently, microfluidic chips (MFCs) have been widely used in biosensors for detecting foodborne pathogens [19] and determining liquid composition [20] as well as conducting cancer research [21], owing to their advantages of convenient manufacture, low cost, and minute sample consumption.

Due to the excellent THz absorption characteristics of MWCNT [12], the transmission spectrum amplitude is small. In the existing literature [1], MWCNTs are usually treated in solid films with micron thickness for research, while the characteristics of MWCNT aqueous dispersion are rarely studied. The MWCNT aqueous dispersion has important applications in the fields of conductive film preparation [22], composite material performance improvement [23], and wearable technology sensors [24]. Thus, MWCNT aqueous dispersion has a certain research value. Microfluidic technology is used to control the thickness of the liquid sample to the order of 100 microns, which greatly reduces the absorption of THz waves by water. It is convenient and feasible to combine THz spectroscopy technology and microfluidic technology to obtain rich information about the THz properties of MWCNT aqueous dispersion. In this study, MWCNT aqueous dispersion and microfluidic technology are combined innovatively to study the THz absorption characteristics of the MWCNT aqueous dispersion under the action of applied electric field (EF) and magnetic field (MF). This also provides a feasible method for studying the THz properties of other THz absorbing materials.
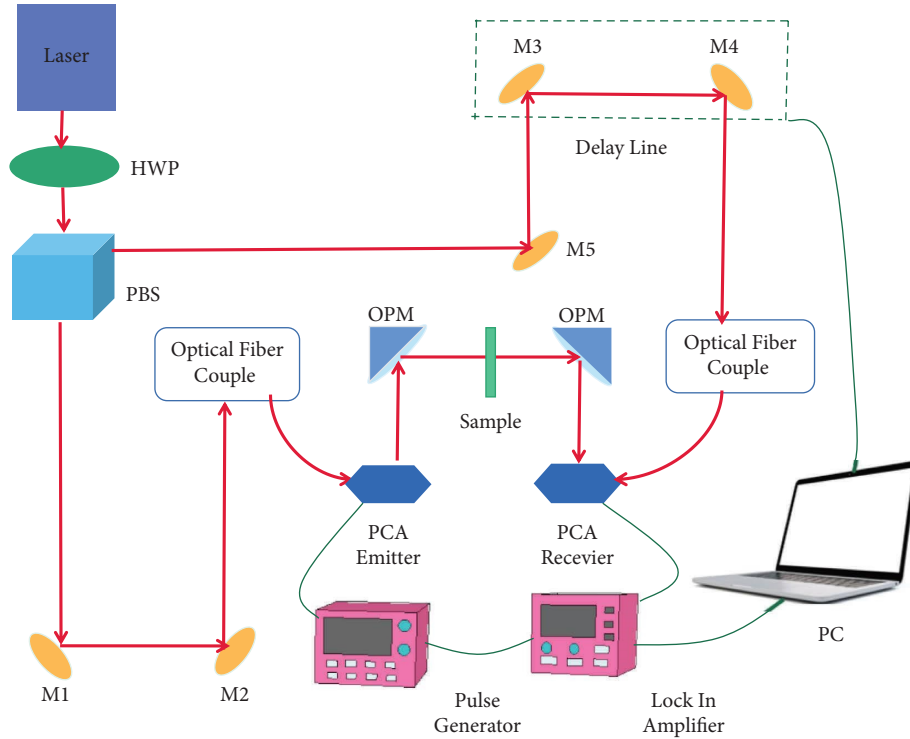
FIGURE 2: Experimental light path diagram. M1-5, reflector; PBS, polarization beam splitter; HWP, half-wave plate; OPM, off-axis parabolic mirror.

2. Experimental Part

2.1. Experimental Light Path. The experimental optical path is shown in Figure 2. The laser is a self-mode-locked fiber femtosecond laser developed by Peking University. Its central wavelength is 1550 nm, the pulse repetition frequency is 100 MHz, the pulse width is 75 fs, and the output power is 130 mW. The laser is divided into two beams through a polarizing prism. A beam of light acts as a pump path and is coupled to a fiber optic photoconductive antenna to generate THz waves; the other serves as a detection path, coupled to another fiber-optic antenna to detect THz waves. The THz wave is focused on the MFC through an off-axis parabolic mirror and then carries information about the MWCNT aqueous dispersion. After being focused by another off-axis parabolic mirror, it is received by the detection antenna and fed to a phase-locked amplifier for amplification. Finally, the data are collected and processed by the computer. The overall photograph of the experimental device with EF applied is shown in Figure 3.

2.2. Manufacturing of the MFCs. In this experiment, a cycloolefin copolymer (COC) is used to make MFCs, and the transmittance of THz waves exceeded 90%, making it an excellent material for MFCs [25]. In the experiment, two pieces of COC with a size of 3 cm × 3 cm × 2 mm are used as substrate and cover, and then, concave regions with a length of 2 cm and a width of 1.5 cm are carved on a 3M double-sided tape with a thickness of 50 μm. Next, a drill bit is used with a diameter of 2 mm to drill two holes that
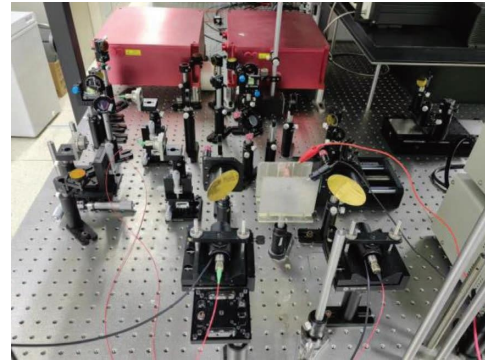
FIGURE 3: An overall photograph of the experimental device with EF applied.

protrude from each end of the concave area. Metal tubes are inserted into each hole to serve as the liquid inlet and outlet. Finally, the double-sided tape is used to adhere the cover to the substrate. The hollow part of the double-sided tape in the middle of the chip is the liquid pool, as shown in Figure 4.

2.3. External EF System. Figure 5 shows the EF system perpendicular to the direction of THz transmission. The high voltage power supply module provides voltage for the plate (DW-P1530-0.5C51, Dongwen High Voltage Power Supply (Tianjin) Co., Ltd.), whose output voltage can be varied between 0 and 15000 V by adjusting the potentiometer.

FIGURE 4: Fabrication of the MFC.
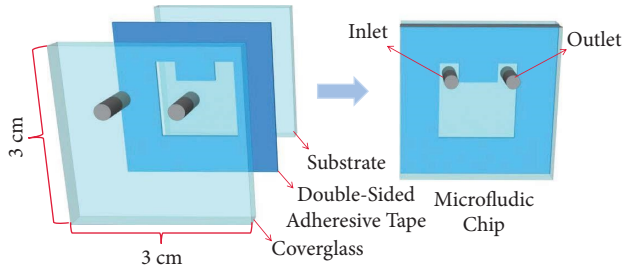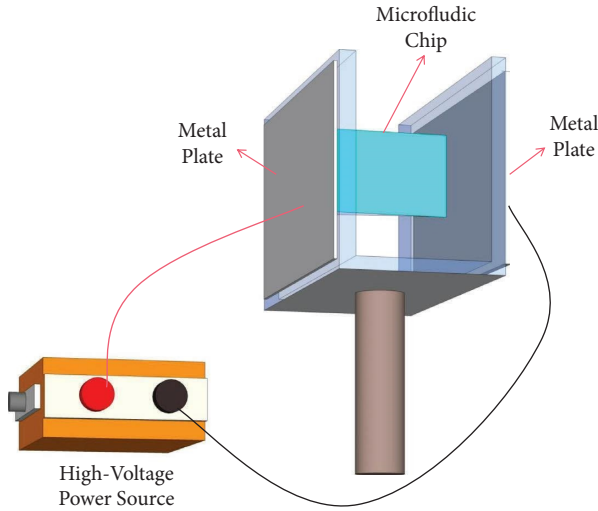

FIGURE 5: Diagram of an EF system.

2.4. External MF System.
The experiment uses two miniature electromagnets to provide the MF. It is powered by the regulated power supply, and the working voltage of the electromagnet is changed by adjusting the output voltage of the regulated power supply (output voltage range: 12–20 V), so as to adjust the strength of MF. The MFC filled with MWCNT aqueous dispersion is placed in different uniform MFs. The THz wave reaches the MFC through a hole in the middle of one electromagnet and then carries the sample information through the hole in the middle of another electromagnet. Finally, the THz wave is detected by the detection antenna. Figure 6 shows a MF system with MF intensity parallel to the direction of THz transmission.

2.5. Data Processing Method.
The absorption coefficient of a sample can be obtained as follows:

$$n(\omega) = 1 + \frac{c}{\omega\,d}\phi(\omega), \tag{1}$$

$$\alpha(\omega) = -\frac{2}{d}\ln\frac{[n(\omega)+1]^2}{4n(\omega)}\left|\frac{E_{\text{sample}}(\omega)}{E_{\text{reference}}(\omega)}\right|, \tag{2}$$

where c denotes the speed of light in a vacuum, $\phi(\omega)$ denotes the phase difference between the sample and reference signals, ω denotes the angular frequency of the signal, d denotes the thickness of the sample, $n(\omega)$ denotes the sample refractive index, $E_{\text{sample}}(\omega)$ and $E_{\text{reference}}(\omega)$ represent the
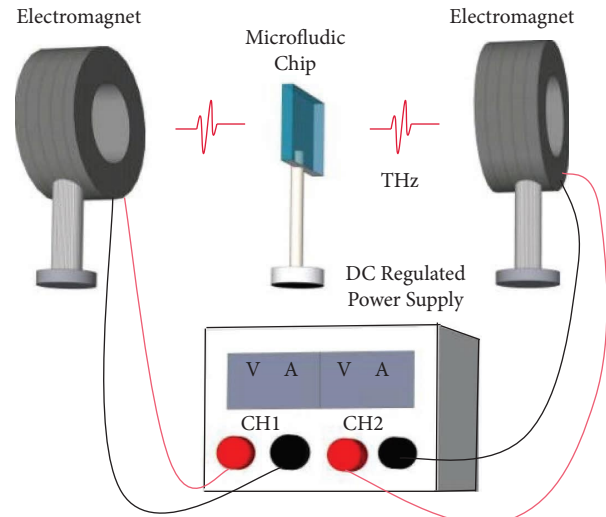

FIGURE 6: Diagram of an MF system.

Fourier transform amplitudes of the sample and reference signals, respectively, and $\alpha(\omega)$ denotes the sample absorption coefficient. Thus, the THz absorption spectra of MWCNT aqueous dispersion under different EF and MF intensities may be obtained.

2.6. Preparation of Samples and Experimental Process.
MWCNTs aqueous dispersion solution at a concentration of 5% was purchased from Suzhou Tianfeng Co., Ltd. The MWCNTs powder is first mixed with water and then undergoes ultrasonic dispersion treatment, and finally, the surfactant PVP is added. The purity of the MWCNT powder used is more than 95%, and the outer diameter of the MWCNT is 15 nm, which is prepared by chemical vapor deposition. Moreover, the mass ratio of MWCNTs to PVP is between 5% and 10%.

The experimental process of this study is as follows. First, without applying an EF and an MF, the MPC without sample injection is put into the experimental optical path to obtain a reference signal. Then, MWCNT aqueous dispersion is injected through the inlet of the MFC until the liquid is discharged from the outlet, whilst ensuring that no bubbles are present in the MFC. Next, the MFC with the sample is placed in the environment under different magnitudes of EF strength or MF strength, and the THz transmission data are acquired via the THz-TDS system. Finally, the data are processed by a computer.

3. Results and Discussion

3.1. THz Spectral Characteristics of MWCNT Aqueous Dispersion under Different EF Intensities.
The MFC filled with MWCNT aqueous dispersion at a concentration of 5% is placed in a THz-TDS system. EF intensities of 500, 1000, 1500, 2000, and 2500 V/cm are applied perpendicular to the THz transmission direction. At each EF intensity, an EF is applied to the sample for 5 minutes, and the time and frequency-domain spectra are obtained using a THz-TDS
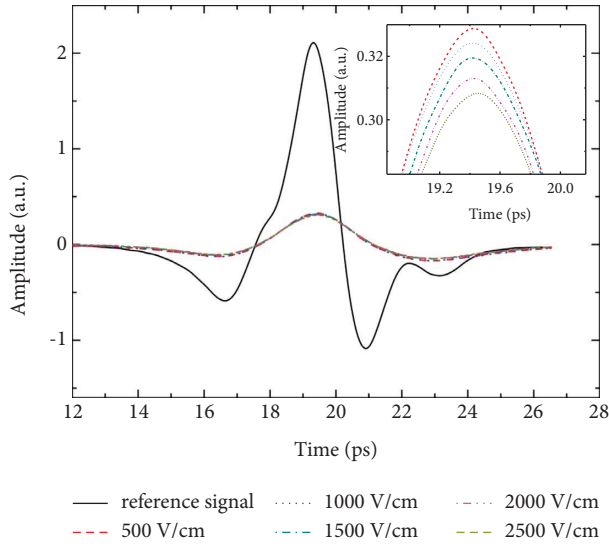
FIGURE 7: THz time-domain spectra of MWCNT aqueous dispersion under different EF intensities.

FIGURE 8: THz frequency-domain spectra of MWCNT aqueous dispersion under different EF intensities.

system. After each measurement, the switch is turned off, and the MFC filled with MWCNT aqueous dispersion is left standing for 10 minutes to restore it to its original state as much as possible [26]. The experimental results are shown in Figures 7–9. The time-domain waveform of the sample is significantly delayed relative to the reference signal, which is obtained by the COC empty chip. This is because the refractive index of the sample differs from that of air. The length of the optical path of THz penetrating the sample increases, and a time delay occurs, which is reflected in the right shift of the peak value of the time-domain spectra. According to the frequency-domain spectra, the spectral intensity of MWCNT aqueous dispersion decreases with an increase in EF intensity. The THz absorption coefficient of MWCNT aqueous dispersion increases with an increase in EF intensity, as shown in Figure 9, which agrees with the changing trend of spectral intensity in the frequency-domain spectra.

Under the action of an external EF, the MWCNT molecules will show an induced dipole moment, and the electric dipole rotates under the action of torque in the external EF, making the electric dipole moment shift toward the external EF direction so that the MWCNT molecules that have been randomly distributed will be aligned in the EF line direction. This finding agrees with the phenomenon observed by Guo et al. [27] that the formation of a long-range CNT structure is induced by EF, that is, the axial elongation of the structure was observed along the EF line direction. Cai et al. [28] found that the transmission intensity of THz increased when pure deionized water stood in an EF, whereas the spectral intensity of MWCNT aqueous dispersion decreased in this study, showing that the change in the transmission intensity of THz was caused by PVP/MWCNT composite particles. Polley et al. [29] revealed that when the outer tube diameter of MWCNT was less than 25 nm, it had a shielding effect on THz waves, and this shielding effect was mainly caused by the THz absorption of
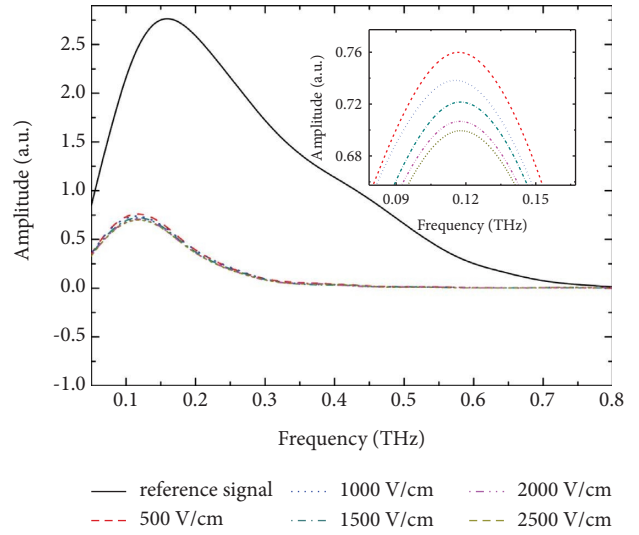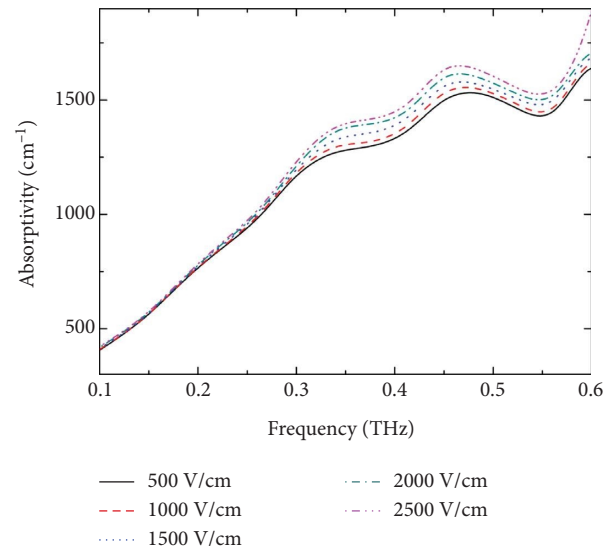

FIGURE 9: THz absorption spectra of MWCNT aqueous dispersion under different EF intensities.

MWCNT. Because the outer diameter of the MWCNT used in this experiment is 15 nm, the THz shielding mechanism of the MWCNT in this experiment is mainly absorption. In addition, Yang et al. [30] found that the combination of surfactants and carbon nanotubes can improve the polarity of carbon nanotubes. With an increase in EF intensity, the intermolecular van der Waals force weakens because of the increase in molecular dispersion of MWCNTs, but the polarization degree of PVP/MWCNT composite particles increases. Therefore, the intermolecular force of PVP/MWCNT composite particles in an EF is mainly an intermolecular interaction of dipoles. Moreover, THz wave absorption is closely related to the change of dipole moment when molecules vibrate. For example, Yan et al. [31] found that the stronger the polarity of the molecule, the greater the change of dipole moment and the peak of the THz

absorption spectrum when it vibrated. Thus, the enhanced THz absorption of MWCNT aqueous dispersion is principally due to the dipole intermolecular vibration. In Figure 9, the absorption curve of MWCNT aqueous dispersion fluctuates in the 0.3–0.6 THz band. In our previous studies [32], the absorption curve of water has a similar fluctuation in the 0.4–0.6 THz band. We believe that the fluctuation of the absorption curve of the MWCNT aqueous dispersion in Figure 9 is mainly affected by the THz absorption of water.

3.2. THz Spectral Characteristics of MWCNT Aqueous Dispersion under Different MF Intensities.
The MFC injected with MWCNT water dispersion is placed in an MF system and tested using a THz-TDS system. The MF around the MFC is changed by changing the voltage. The MF intensities are 24, 30, 36, and 40 mT, and data are collected after each MF was applied to the sample for 3 minutes at each MF intensity. After each measurement, we turn off the switch and let the MFC stand for 10 minutes to restore it to its original state as much as possible. According to the time-domain spectra, as shown in Figure 10, the THz pulse moves slightly to the right. Figures 11 and 12 indicate the enhanced absorption of THz waves by MWCNT aqueous dispersion with an increase in the external MF intensity.

Sun et al. [33] used a weak curing MF (less than 0.7 T) to induce MWCNTs arranged in polymer composites to obtain a novel flexible strain sensor with an anisotropic structure, indicating that the orientation and extension of MWCNTs are parallel to the MF direction under the action of externally strengthened MF. Because of the magnetic anisotropy of MWCNTs, the orientation of MWCNTs in a solution is parallel to the MF direction and THz transmission direction under the action of an external MF. A THz absorption spectrum is a concentrated representation of intramolecular interactions of atoms and atomic groups, intermolecular hydrogen bonds, and van der Waals forces [34]. The change in the intermolecular hydrogen bond network will affect the molecular vibration mode and its THz absorption intensity [35]. With an increase in the MF intensity, the dispersion degree of the originally agglomerated or entangled MWCNT molecules and the binding sites of MWCNT molecules and surfactants increase. The interaction between the surfactant hydrophobic chain and MWCNT sidewall and the hydrogen bond between water and the carbonyl group on the PVP side chain are enhanced by an increase in the binding sites and reaction density, thereby enhancing the THz absorption. In addition, the MF can stimulate the generation of non-equilibrium carriers to raise the Fermi level to a higher conduction band and thus promote THz absorption [36]. The higher the MF strength, the more nonequilibrium carriers produced by the MWCNTs. That is why the absorption coefficient of MWCNT aqueous dispersion increases with the increase of MF intensity.

3.3. THz Spectral Characteristics of MWCNT Aqueous Dispersion under the Same MF Intensity and Different Action Time.
With the MF intensity at 40 mT, the sample is administered for 30 minutes, and the experimental data are
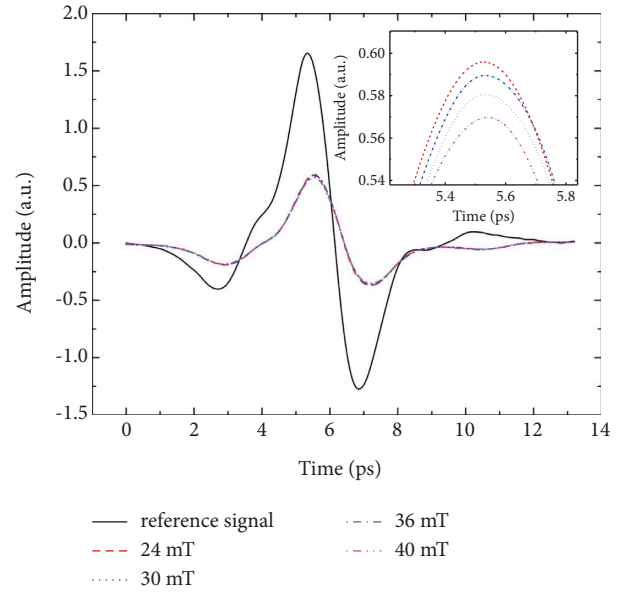

FIGURE 10: THz time-domain spectra of MWCNT aqueous dispersion under different MF intensities.
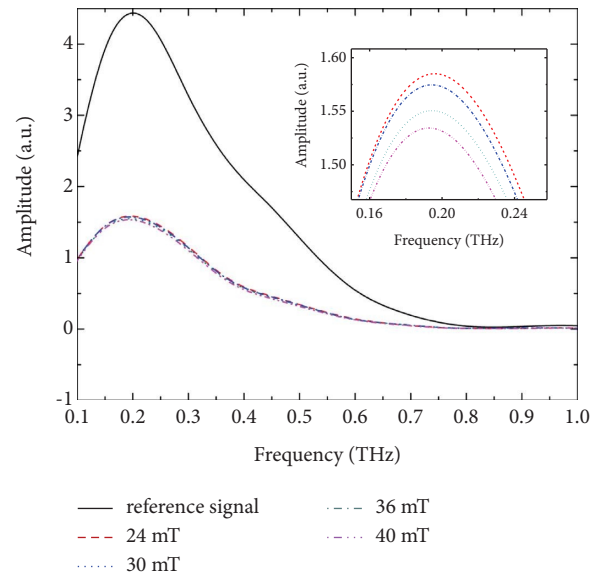

FIGURE 11: THz frequency-domain spectra of MWCNT aqueous dispersion under different MF intensities.

recorded at 6, 14, 22, and 30 minutes. Figures 13–15 show the spectra of the time-domain, frequency-domain, and absorption coefficient, respectively. The increase in the standing MF action time is consistent with the increase in the MF intensity.

With an increase in the time of MWCNT aqueous dispersion under the same MF intensity, more MWCNT molecules have the sufficient reaction time to respond to the external MF, so MWCNTs can be more evenly distributed in the aqueous solvent. The excess MWCNTs in the suspension will form connections between the arranged MWCNT bundles, thereby forming a branching network [27]. This makes it difficult for THz waves to penetrate,
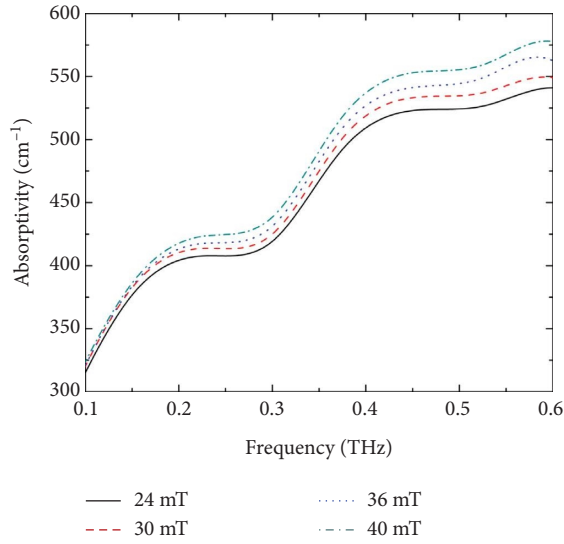
Figure 12: THz absorption spectra of MWCNT aqueous dispersion under different MF intensities.
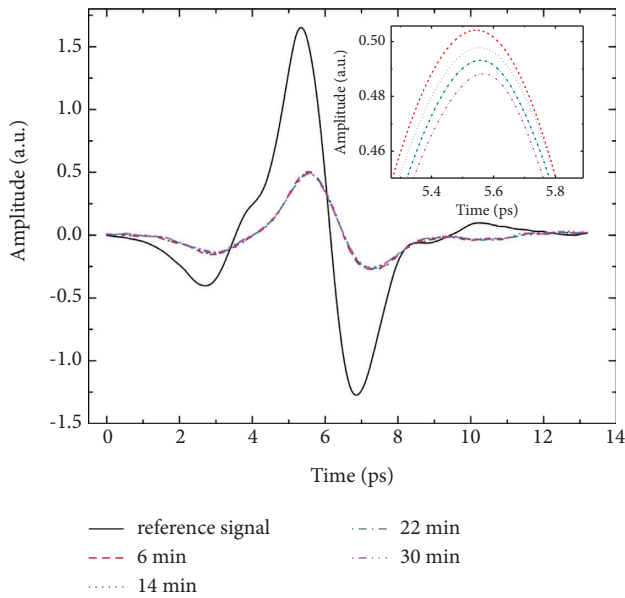

Figure 14: THz frequency-domain spectra of MWCNT aqueous dispersion under same MF intensity and different time.

Figure 13: THz time-domain spectra of MWCNT aqueous dispersion under same MF intensity and different time.
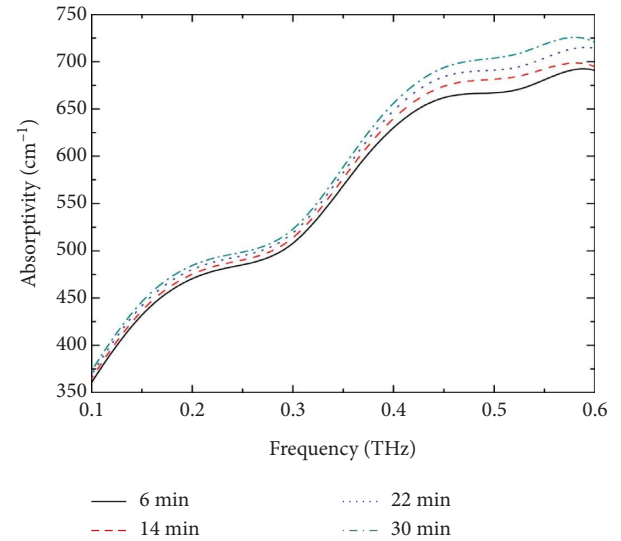
Figure 15: THz absorption spectra of MWCNT aqueous dispersion under same MF intensity and different time.

resulting in increased absorption with time. In addition, with the increase of time, the higher the nonequilibrium carrier density, which also leads to the increase of THz absorption [36]. THz absorption is closely related to frequency. Pan et al. [37] found that the absorption curve of graphene foam in the frequency band of 0.1–1.6 THz showed a gradient upwards trend with an increasing frequency. In this study, the absorption curve of MWCNT aqueous dispersion also shows a gradient rising trend with the increase of frequency in the 0.1–0.6 THz band under the stimulation of MF, as shown in Figures 12 and 15. This phenomenon is probably determined by the characteristics of THz waves.
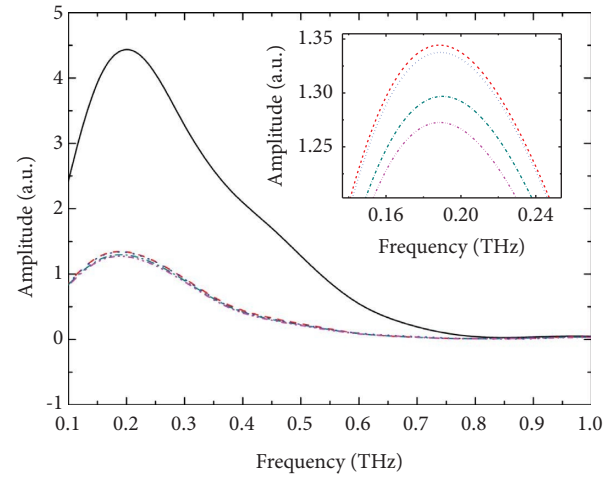
4. Conclusion

A COC MFC is combined with a THz-TDS system in this study. We find that the THz spectral intensity of MWCNT aqueous dispersion decreases with an increase in EF intensity, mainly because of the enhanced dipole–dipole interaction between MWCNT molecules. Moreover, the THz spectrum intensity of MWCNT aqueous dispersion decreases with an increase in MF intensity, mainly because of the enhanced hydrogen bond between water and the carbonyl group on the PVP side chain as well as the interaction between the surfactant hydrophobic chain and the MWCNT sidewall. Finally, the effects of different MF action times on the THz absorption characteristics of MWCNT aqueous

dispersion are studied. The experimental phenomenon is the same as that when the MF intensity increases, which may be related to the branching network formed between MWCNTs. In this study, with the increase of EF intensity, MF intensity, and MF action time, the THz spectral intensity of MWCNT aqueous dispersion decreased and the absorption coefficient increased. This introduces a theoretical foundation for the application of MWCNT aqueous dispersion in the improvement of composite properties. Moreover, this article provides a feasible method for studying THz characteristics and microstructure of MWCNT aqueous dispersion and THz absorbing materials.

Data Availability

The data used to support the findings of this study are available from the corresponding author upon request.

Conflicts of Interest

The authors declare that they have no conflicts of interest.

Authors' Contributions

All authors contributed to the theoretical analysis, calculations, experiment, and preparation of the manuscript.

Acknowledgments

References

[1] H. Lamela, E. Dadrasnia, F. Garet, M. B. Kuppam, and J.-L. Coutaz, "Carbon nanotube terahertz spectroscopy: study of absorption and dispersion properties of SWNT and MWNT," *Proceedings of the International Society for Ootical Engineering*, vol. 8101, pp. 1–7, 2011.

[2] H. Masanori, "Development and future prospects of terahertz technology," *Japanese Journal of Applied Physics*, vol. 81, no. 4, pp. 271–283, 2012.

[3] J. F. Federici, J. Ma, and L. Moeller, "Review of weather impact on outdoor terahertz wireless communication links," *Nano Communication Networks*, vol. 10, no. 10, pp. 13–26, 2016.

[4] E. Heinz, T. May, D. Born et al., "Passive submillimeter-wavestand-off video camera for security applications," *Journal of Infrared, Millimeter and Terahertz Waves*, vol. 31, no. 11, pp. 1355–1369, 2010.

[5] F. Chen, Y. Cheng, and H. Luo, "Temperature tunable narrow-band terahertz metasurface absorber based on InSb micro-cylinder arrays for enhanced sensing application," *IEEE Access*, vol. 8, no. 1, pp. 82981–82988, 2020.

[6] W. Shui, J. Li, H. Wang et al., "Ti₃C₂Tx MXene sponge composite as broadband terahertz absorber," *Advanced Optical Materials*, vol. 8, no. 21, Article ID 2001120, 2020.

[7] F. Chen, Y. Cheng, and H. Luo, "A broadband tunable terahertz metamaterial absorber based on single-layer complementary gammadion-shaped graphene," *Materials*, vol. 13, no. 4, p. 860, 2020.

[8] W. Li and Y. Cheng, "Dual-band tunable terahertz perfect metamaterial absorber based on strontium titanate (STO) resonator structure," *Optics Communications*, vol. 462, Article ID 125265, 2020.

[9] Y. Cheng, J. Liu, F. Chen, H. Luo, and X. Li, "Optically switchable broadband metasurface absorber based on square ring shaped photoconductive silicon for terahertz waves," *Physics Letters A*, vol. 402, Article ID 127345, 2021.

[10] Y. Cheng, Z. Li, and Z. Cheng, "Terahertz perfect absorber based on InSb metasurface for both temperature and refractive index sensing," *Optical Materials*, vol. 117, Article ID 111129, 2021.

[11] Y. Cheng, H. Zhao, and C. Li, "Broadband tunable terahertz metasurface absorber based on complementary-wheel-shaped graphene," *Optical Materials*, vol. 109, Article ID 110369, 2020.

[12] Z. Huang, H. Chen, S. Xu et al., "Graphene-based composites combining both excellent terahertz shielding and stealth performance," *Advanced Optical Materials*, vol. 6, no. 23, pp. 1801165–1801168, 2018.

[13] G. V. Gorokhov, D. S. Bychanok, P. P. Kuzhir et al., "Creation of metasurface from vertically aligned carbon nanotubes as versatile platform for ultra-light THz components," *Nanotechnology*, vol. 31, no. 25, pp. 255703–255708, 2020.

[14] B. Munkhbayar, M. Bat-Erdene, B. Choi, T. Joun, H. Chung, and H. Jeong, "Grinding effect of rotation speed on the surface changes of multi-walled carbon nanotubes and their dispersion ability," *Asian Journal of Chemistry*, vol. 25, no. 2, pp. 883–890, 2013.

[15] B. Wang, S. Liu, Y. Zhu, and S. Ge, "Influence of polyvinyl pyrrolidone on the dispersion of multi-walled carbon nanotubes in aqueous solution," *Russian Journal of Physical Chemistry A*, vol. 88, no. 13, pp. 2385–2390, 2014.

[16] S. Iijima, "Helical microtubules of graphitic carbon," *Nature*, vol. 354, no. 6348, pp. 56–58, 1991.

[17] L. Forró and C. Schönenberger, "Physical properties of multi-wall nanotubes," *Carbon Nanotubes*, vol. 80, pp. 329–391, 2001.

[18] J. Qiu, G. Wang, and J. Shang, "Multi-walled carbon nanotubes modified by poly (vinylpyrrolidone)," *Acta Polymerica Sinica*, vol. 7, no. 4, pp. 327–331, 2007.

[19] X. Zhao, M. Li, and Y. Liu, "Microfluidic-based approaches for foodborne pathogen detection," *Microorganisms*, vol. 7, no. 10, p. 381, 2019.

[20] D. Mondal, N. K. Tiwari, and M. J. Akhtar, "Microwave assisted non-invasive microfluidic biosensor for monitoring glucose concentration," in *Proceedings of the 2018 IEEE Sensors*, pp. 1–4, NewDelhi, India, October 2018.

[21] P. K. Chaudhuri, M. Ebrahimi Warkiani, T. Jing, K. Kenry, and C. T. Lim, "Microfluidics for research and applications in oncology," *The Analyst*, vol. 141, no. 2, pp. 504–524, 2016.

[22] R. Jung, H. S. Kim, Y. Kim, S. M. Kwon, H. S. Lee, and H. J. Jin, "Electrically conductive transparent papers using multiwalled carbon nanotubes," *Journal of Polymer Science Part B: Polymer Physics*, vol. 46, no. 12, pp. 1235–1242, 2008.

[23] O. A. Mendoza Reales, P. Duda, and R. Dias Toledo Filho, "Effect of a carbon nanotube/surfactant aqueous dispersion on the rheological and mechanical properties of portland cement pastes," *Journal of Materials in Civil Engineering*, vol. 30, no. 10, Article ID 04018259, 2018.

[24] L. Liu, M. Wu, Q. Wu, J. Liu, J. Yang, and J. Zhang, "Conductive, superhydrophobic, and microwave-absorbing cotton fabric by dip-coating of aqueous silk nanofibers stabilized

mwcnts and octadecanoyl chain bonding," *Cellulose*, vol. 29, no. 8, pp. 4687–4701, 2022.

[25] X. Fang, Y. Xuan, and Q. Li, "Investigation on the optical characteristic of magnetic fluid film in the presence of an external MF," *Journal of Engineering* Ermophysics*, vol. 30, no. 8, pp. 1386–1388, 2009.

[26] X. Y. Zhao, G. Y. Wang, S. Y. Shao et al., "Terahertz characteristics of magnetic fluid based on microfluidic technology," *International Journal of Optics*, vol. 2021, Article ID 5599185, 8 pages, 2021.

[27] Z. Guo, J. A. Wood, K. L. Huszarik, X. Yan, and A. Docoslis, "AC electric field-induced alignment and long-range assembly of multi-wall carbon nanotubes inside aqueous media," *Journal of Nanoscience and Nanotechnology*, vol. 7, no. 12, pp. 4322–4332, 2007.

[28] Y. Cai, J. H. Wang, Z. C. Bai, B. Su, and C. L. Zhang, "Terahertz transmission characteristics of water induced by electric field," *Spectroscopy and Spectral Analysis*, vol. 41, no. 6, pp. 1683–1687, 2021.

[29] D. Polley, K. Neeraj, A. Barman, and R. K. Mitra, "Diameter-dependent shielding effectiveness and terahertz conductivity of multiwalled carbon nanotubes," *Journal of the Optical Society of America B*, vol. 33, no. 12, pp. 2430–2436, 2016.

[30] B. Yang, D. Y. Guo, P. R. Lin et al., "Hydroxylated multi-walled carbon nanotubes covalently modified with tris (hydroxypropyl) phosphine as a functional interlayer for advanced lithium-sulfur batteries," *Angewandte Chemie*, vol. 61, no. 28, Article ID e202204327, 2022.

[31] H. L. Yan, Y. Q. Cheng, K. L. Wang et al., "Terahertz wave absorption for alkylcyclohexyl-isothiocyanatobenzene liquid crystal materials," *Acta Physica Sinica*, vol. 68, no. 11, Article ID 116102, 2019.

[32] H. M. Jiang, Q. J. Li, Y. Shen et al., "Terahertz spectral characteristics of konjac gum determined via microfluidic technology," *International Journal of Optics*, vol. 2022, Article ID 1358756, 7 pages, 2022.

[33] R. X. Sun, L. X. Gao, F. Q. Liu et al., "Magnetically induced robust anisotropic structure of multi-walled carbon nanotubes/Ni for high-performance flexible strain sensor," *Carbon*, vol. 194, pp. 185–196, 2022.

[34] F. Yan, W. Li, and Z. C. Wang, "Terahertz vibration modes of aminoacid functional groups," *Spectroscopy and Spectral Analysis*, vol. 40, no. 2, pp. 397–402, 2020.

[35] M. Heyden, J. Sun, S. Funkner et al., "Dissecting the THz spectrum of liquid water from first principles via correlations in time and space," *Proceedings of the National Academy of Sciences*, vol. 107, no. 27, pp. 12068–12073, 2010.

[36] R. Cheng, Y. Zhou, H. Liu et al., "Tunable graphene-based terahertz absorber via an external magnetic field," *Optical Materials Express*, vol. 10, no. 2, pp. 501–512, 2020.

[37] J. Pan, H. Hu, Z. Li, J. Mu, Y. Cai, and H. Zhu, "Recent progress in two-dimensional materials for terahertz protection," *Nanoscale Advances*, vol. 3, no. 6, pp. 1515–1531, 2021.